
Locally Adaptive Conformal Inference for Operator Models

Trevor A. Harris *

Department of Statistics
University of Connecticut
Storrs, CT 15213
trevor.a.harris@uconn.edu

Yan Liu

Meta Platforms Inc
New York City, NY 10003
yan15illinois@gmail.com

Abstract

Operator models are regression algorithms for functional data and have become a key tool for emulating large-scale dynamical systems. Recent advances in deep neural operators have dramatically improved the accuracy and scalability of operator modeling, but lack an inherent notion of predictive uncertainty. We introduce Local Spectral Conformal Inference (LSCI), a new framework for locally adaptive, distribution-free uncertainty quantification for neural operator models. LSCI uses projection-based depth scoring and localized conformal inference to generate function-valued prediction sets with statistical guarantees. We prove approximate finite-sample marginal coverage under local exchangeability, and demonstrate significant gains in adaptivity and coverage across synthetic and real-world operator learning tasks.

1 Introduction

An operator is a map $\Gamma : \mathcal{F} \mapsto \mathcal{G}$ between two function spaces \mathcal{F} and \mathcal{G} . Given a function f as input, an operator Γ returns another function $g = \Gamma(f)$. An operator model, then, is a parameterized operator $\Gamma_\theta : \mathcal{F} \mapsto \mathcal{G}$ that is trained to predict functions $g \in \mathcal{G}$ given functions $f \in \mathcal{F}$. As in ordinary regression, we learn an operator model's parameters $\theta \in \Theta$ by minimizing a function valued loss $\mathcal{L} : \Theta \times (\mathcal{F}, \mathcal{G}) \mapsto \mathbb{R}$. Many scientific and engineering problems can be cast as operator learning problems. Recent works include partial differential equation (PDE) approximation [24] and closure modeling [41], weather forecasting [38] and climate downscaling [17], medical imaging [30], and image super-resolution [48].

Early approaches to operator modeling used linear operator models to infer statistical relationships between functional covariates and functional response variables [39, 5, 52, 50, 16]. Linear models typically take one of two forms [47]

$$\Gamma_\theta(f)(t) = \beta_0(t) + \beta_1(t)f(t) \quad \text{or} \quad \Gamma_\theta(f)(t) = \alpha_0(t) + \int_D \beta_1(t, s)f(s)ds \quad (1)$$

where β_1 and α_1 act as weight functions, β_0 and α_0 as bias functions. The response $g \in \mathcal{G}$ is modeled pointwise as $g(t) = \Gamma_\theta(f)(t) + \epsilon(t)$, where $\epsilon(t)$ is an assumed error process, such as a Gaussian process. Non-linear extensions using higher-order polynomial terms include [51, 12, 11, 31, 43].

A recent innovation in non-linear operator modeling are the Neural Operator (NOs) models, which mimic the structure of deep neural networks [9, 28, 6, 37]. Neural operators sequentially build up the operator Γ_θ through a sequence of non-linear kernel integrations. An L -layer neural operator is

*<https://github.com/trevor-harris/LSCI>

defined as $\Gamma_\theta = Q \circ K_L \circ \dots \circ K_1 \circ R$, where R and Q are linear projection operators and each K_l is a kernel integration [19, 20]. Each non-linear kernel integrations is defined as

$$K_l(v)(t) = \sigma \left(W_l v(t) + b_l(t) + \int_D k^l(t, s) v(s) ds \right), \quad (2)$$

where v is the output of K_{l-1} , σ is a point-wise activation function, W_l and b_l are weight and bias matrices, and k^l is a neural network [24]. Neural operators have been shown to approximate the solutions of non-linear PDEs, such as Navier-Stokes and Darcy’s equations, at a fraction of the cost of numerical methods [24, 7, 46, 21, 4, 20]. Other applications include large-scale weather forecasting [38], climate model downscaling [17], 3D automotive aerodynamic simulation [25], and carbon capture storage reservoir pressure buildup [49].

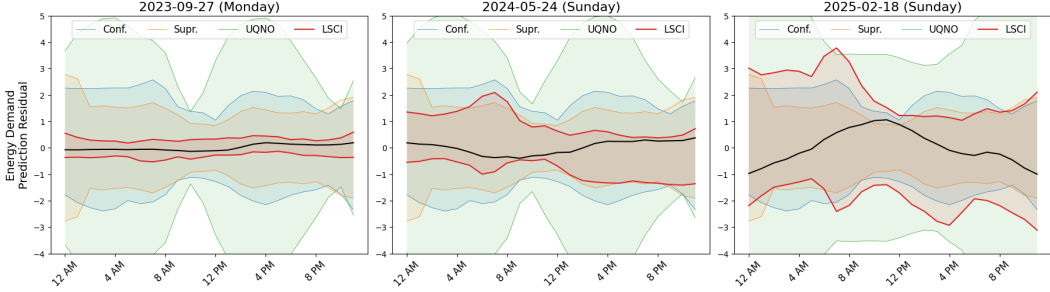


Figure 1: Example prediction sets using three baseline methods (Section 3.5) and the proposed method (LSCI) on Energy Demand data (Section 4.2). Three examples of prediction sets for different levels of residual variability.

In many domains where NOs are currently being applied, such as in weather and climate modeling, precise uncertainty quantification (UQ) is critical. However, unlike statistical operator models, NOs do not contain an inherent notion of uncertainty because they lack an explicit probabilistic model. This severely limits their utility and trustworthiness for high stakes applications and rigorous scientific discovery. Therefore, we propose a new statistically rigorous uncertainty quantification technique for NO models, based on locally adaptive conformal inference [44, 22], called Local Spectral Conformal Inference (LSCI).

Building on recent works for conformal inference for functional data [23, 10, 29, 32, 35] and local conformal inference [15, 13], we introduce a new functional conformity measure called local Φ -scores that allows us to construct locally adaptive, and statistically valid, prediction sets for operator models. We show that conformalization with local Φ -scores results in statistically exact prediction sets that are highly adaptive to local variations (Figure 1). To make LSCI prediction sets practical, we further introduce a simple sampling procedure to generate prediction ensembles and prediction bands.

2 Background

Conformal Inference Conformal inference is a general family of procedures for imbuing arbitrary prediction algorithms with exact, finite-sample, uncertainty quantification [44, 22]. Given a prediction algorithm $\Gamma_\theta : \mathcal{F} \mapsto \mathcal{G}$, we first train the model on the training dataset $\mathcal{D}_{tr} = \{(f_s, g_s)\}_{s=1}^m$ where $f_s \in \mathcal{F}$ and $g_s \in \mathcal{G}$. Then, given separate calibration data $\mathcal{D}_{cal} = \{(f_t, g_t)\}_{t=1}^n$, and a test point f_{n+1} , a conformal procedure generates a prediction set $C_\alpha(f_{n+1}) \subset \mathcal{G}$ such that

$$P(g_{n+1} \in C_\alpha(f_{n+1})) \geq 1 - \alpha \quad (3)$$

under the key assumption that (f_t, g_t) for $t \in 1, \dots, n + 1$ form an exchangeable sequence. The prediction set $C_\alpha(f_{n+1})$ depends on the model Γ_θ , although we omit explicit conditioning for notational convenience. In the standard split, or *inductive*, conformal procedure we define $C_\alpha(f_{n+1}) = \Gamma_{\hat{\theta}}(f_{n+1}) \pm k_n$, where k_n is the $\lceil (1 - \alpha)(n + 1) \rceil / n$ quantile of the calibration residual scores $S(f_t, g_t) = \|g_t - \Gamma_{\hat{\theta}}(f_t)\|_2$.

Adaptive Conformal Inference The fixed form of the prediction sets, $\pm k_n$, prevents C_α from adapting to heterogeneity in the data (Figure 1), a feature present in many real-world datasets but

dis-allowed under pure exchangeability. Adaptive conformal inference methods attempt to circumvent this issue by either introducing adaptive scoring rules, localization procedures, or through quantile regression based estimators (Section 3.5). Our proposal is based on localization, which has been shown to strongly improve over adaptive scoring rules and quantile regression in univariate tasks [13, 15, 2].

3 Local Spectral Conformal Inference for Operators

Let $\Gamma_\theta : \mathcal{F} \mapsto \mathcal{G}$ denote an operator model from \mathcal{F} to \mathcal{G} . We assume that $\mathcal{F}, \mathcal{G} \subset \mathcal{L}^2(\Omega)$, the space of square integrable functions, i.e., $\int_\Omega f(x)^2 dx < \infty$, on the compact domain $\Omega \subset \mathbb{R}^p$, $p \geq 1$. Let $\mathcal{D}_{tr} = \{(f_s, g_s)\}_{s=1}^m$ denote a sequence of m training regression pairs, and let $\mathcal{D}_{cal} = \{(f_t, g_t)\}_{t=1}^n$ denote n calibration pairs. We use different indexing notations, s and t , to emphasize that \mathcal{D}_{tr} and \mathcal{D}_{cal} are disjoint sets. Finally, let $\alpha \in (0, 1)$ denote a confidence level, let f_{n+1} denote the new test function, and let g_{n+1} denote the unobserved target function.

Our goal is to construct a prediction set $C_\alpha(f_{n+1})$ such that $P(g_{n+1} \in C_\alpha(f_{n+1})) \geq 1 - \alpha$ and such that $C_\alpha(f_{n+1})$ is *locally adaptive* to changes in the conditional distribution of $g_{n+1} \mid f_{n+1}$, such as shape or variance changes. We formalize this processing by assuming that $g_t \mid f_t$ can be additively decomposed as

$$g_t \mid f_t = \Gamma(f_t) + r_t, \quad (4)$$

where $\Gamma : \mathcal{F} \mapsto \mathcal{G}$ is an unknown operator and $r_t \in (r_t)_{t \in \mathcal{T}}$ is locally exchangeable error process [8]. Local exchangeability relaxes exchangeability to allow the distribution of r_t to evolve smoothly over the indices $t \in \mathcal{T}$ (Section A.1). We denote the distribution of each r_t as $P_t \in \mathcal{P}(\mathcal{G})$ and the marginal distribution of $(r_t)_{t \in \mathcal{T}}$ as $P \in \mathcal{P}(\mathcal{G})$. In addition to relaxing full exchangeability, assuming local exchangeability allows us to consistently estimate projections of P_t and provide an exact coverage guarantee for our conformal inference procedure (Section 3.3).

Because P_t is a distribution over functions, we cannot directly estimate it as in [8, 13, 15], who used locally weighted empirical distributions to perform local conformal inference. Instead, we will use a classic robust statistics called data depth to characterize the level sets of P_t , and hence $g_{n+1} \mid f_{n+1}$, which will allow us to construct conformal prediction regions directly in function space.

We first review Φ -depths [34], a functional data depth family, and show how Φ -depths define families of local scoring rules, called local Φ -scores. The local Φ -scores allow us to generate “typical sets” of any residual function $r_{n+1} = g_{n+1} - \Gamma_\theta(f_{n+1})$, which circumscribe its variability within a fixed confidence level. We then show that these typical sets constitute exact conformal prediction sets and introduce a sampling procedure to approximate them in practice.

3.1 Φ -depth

Data depth is a classical robust statistics technique for estimating medians and quantile-like quantities of multivariate and functional distributions [26, 53]. There are many depth notions for functional data, including integrated and infimum depths [34, 33], norm depths [53], band depths [27], and shape depths [14]. Let $\mathcal{H} \subset \mathcal{L}^2(D)$ denote a generic function space, $h \in \mathcal{H}$ an element of \mathcal{H} , and $P \in \mathcal{P}(\mathcal{H})$ a probability measure on \mathcal{H} . A general depth function $d : \mathcal{H} \times \mathcal{P} \mapsto [0, 1]$ measures the “outlyingness” of an observation h with respect to a distribution P on a scale from 0 (infinitely outlying) to 1 (centroid of P).

Φ -depths Φ -depths, or infimum depths, are a special class of projection-based functional depth measures that are robust and computationally efficient [34], and, as we show, highly amenable to localization. Let Φ denote any continuous linear function class so that any element $\phi \in \Phi$ is a continuous linear function $\phi : \mathcal{H} \mapsto \mathbb{R}^d$, i.e. a projection function. The Φ -depth corresponding to Φ is defined as

$$D^\Phi(h \mid P) = \inf_{\phi \in \Phi} D(\phi(h) \mid \phi(P)) \quad (5)$$

where $\phi(P)$ denotes the pushforward measure of P under ϕ , and D is a multivariate depth function [26, 53]. We will generally take $\phi(\cdot)$ to be a univariate projection ($d = 1$) and use a univariate depth such as the univariate Tukey depth [36]. As shown in [34], Φ -depths are non-degenerate in function spaces, affine equivariant, robust to outliers, and continuously and monotonically decrease from the

centroid of P . Thus, Φ -depths can be used to define proper orderings of functional data from the center outwards, i.e. from most central ($D^\Phi = 1$) to least central ($D^\Phi = 0$).

Central regions Because Φ -depths induce proper center-out orderings of the data, they can be used to define central regions of the distribution P . An empirical level $\alpha \in (0, 1)$ central region contains the inner $(\alpha \times 100)\%$ observations closest to the centroid of P and is defined as

$$D_\alpha^\Phi(P) = \{h : D^\Phi(h | P) \geq Q_{1-\alpha}(D^\Phi(h | P))\}, \quad (6)$$

where $Q_{1-\alpha}(\cdot)$ is the empirical quantile function. Φ -depths induce nested, convex central regions that monotonically increase as a function of α [34]. Assuming P is unimodal and convex, the central regions will converge to the true central regions as the size of the calibration set goes to infinity, and thus reflect the location, scale, and shape of P . Therefore, Φ -depths give us a simple and convenient characterization of P .

Projection class Φ -depths inextricably depend on the projection class, Φ , which acts to project functional data onto univariate, or multivariate, slices of the distribution. As shown in [34], the projection family Φ can be fixed, data-driven, or even completely random. Fixed projection operators such as Fourier bases, Wavelet bases, and Spline bases are computationally efficient, while data-driven projections such as functional principle components [39] allow for highly compact representations. As we show in Table 4.1, the exact slicing mechanism has little effect on the marginal coverage.

3.2 Method

The central premise of our approach is that $g | f \sim \Gamma(f) + r$ with $(r_t)_{t \in \mathcal{T}}$ locally exchangeable [8], so that new residuals $r_{n+1} \in (r_t)_{t \in \mathcal{T}}$ are locally exchangeable with the calibration residuals r_1, \dots, r_n . Under this assumption, we can evaluate the conformity of any $r \in \mathcal{G}$ with respect to G_{n+1} given only the calibration data \mathcal{D}_{cal} and the new covariate function f_{n+1} . We first introduce a new class of local conformal scoring rules, called local Φ -scores, to efficiently compute the conformity of $r \in \mathcal{G}$ with respect to G_{n+1} .

Local Φ -scoring We first train the operator model $\Gamma_\theta : \mathcal{F} \mapsto \mathcal{G}$ on the training dataset \mathcal{D}_{tr} , so that we can work purely on the residual process $r_t = g_t - \Gamma_{\hat{\theta}}(f_t)$. The calibration residuals r_1, \dots, r_n , and unknown test residual r_{n+1} , are assumed to be locally exchangeable with individual distributions P_1, \dots, P_n, P_{n+1} and marginal distribution P (Section 3). Let Φ denote our chosen univariate projection class, either fixed, random, or data driven, and let $\phi \in \Phi$ be a linear function $\phi : \mathcal{G} \mapsto \mathbb{R}$. We define a Φ -dependent local scoring rule $S : \mathcal{G} \times \mathcal{P} \mapsto \mathbb{R}$ as the *local Φ -depth*

$$S^\Phi(r, P_{n+1}) = D^\Phi(r | P_{n+1}) = \inf_{\phi \in \Phi} D(\phi(r) | \phi(P_{n+1})), \quad (7)$$

where $r = g - \Gamma_{\hat{\theta}}(f)$. That is, the local conformity score of any function $r \in \mathcal{G}$ is its Φ -depth under P_{n+1} , the distribution of r_{n+1} . Ordinarily, this depth would be impossible to compute since r_{n+1} and P_{n+1} are not observed and P_{n+1} is a distribution over functions, and, thus, not possible to directly estimate. However, because we use Φ -depths with *univariate* projections, this depth is not only computable, it is also computationally efficient to evaluate. This is because we only need to estimate the univariate marginal distributions of P_{n+1} along each projection $\phi \in \Phi$, denoted $\phi(P_{n+1})$.

Estimating projected distributions Estimating univariate distributions in non-exchangeable settings is well established in the conformal literature [13, 15, 2]. The residual distribution $\phi(P_{n+1})$ is assumed to vary slowly as a function of time $t \in \mathcal{T}$. The standard locally weighted empirical measure of $\phi(P_{n+1})$ is

$$\hat{\phi}(P_{n+1}) = \sum_{t=1}^n w_t \delta(\phi(r_t)) + w_{n+1} \delta(\infty), \quad (8)$$

where the weights $\{w_t\}_{t=1}^{n+1}$ are based on a localization kernel $H : \mathcal{F} \times \mathcal{F} \mapsto \mathbb{R}$ that measures the similarity of f_t and f_{n+1} . For example $H(f_t, f_{n+1}) = \exp(-\lambda \|f_t - f_{n+1}\|_\infty)$, where $\lambda \geq 0$ is a bandwidth parameter controlling the degree of localization, and $w_t = \text{softmax}(H(f_t, f_{n+1}))$. [15] showed that marginal coverage under local empirical measures can be guaranteed if we localize around \tilde{f}_{n+1} , a statistical knock-off of f_{n+1} , instead of f_{n+1} directly. We employ the knock-off strategy for computing the localization weights by adding a small noise to f_{n+1} .

Given the local empirical measures (Equation 8), local Φ -depths can be computed extremely efficiently without ever having to know P_{n+1} . In fact, because the projections $\phi \in \Phi$ are all independent, each projection can be computed in parallel to reduce the overall compute time. Furthermore, the localization weights can be computed ahead of time, because they are re-used for each projection.

Local Conformal Prediction Sets We take the $\lceil(1 - \alpha)(n + 1)\rceil$ *smallest* value of the local calibration scores $S^\Phi(f_1, g_1), \dots, S^\Phi(f_n, g_n)$ as our f_{n+1} dependent threshold, $q_{1-\alpha}(f_{n+1})$. The quantity $q_{1-\alpha}(f_{n+1})$ defines a central region of the local residual distribution G_{n+1} ,

$$D_\alpha^\Phi(f_{n+1}) = \{r \in \mathcal{G} : D^\Phi(r \mid G_{n+1}) \geq q_{1-\alpha}(f_{n+1})\}, \quad (9)$$

which contains, at least, the inner most $(1 - \alpha) \times 100\%$ of the data relative to G_{n+1} . To form a prediction set for $g_{n+1} = \Gamma_{\hat{\theta}}(f_{n+1}) + r$, we simply shift the $D_\alpha^\Phi(f_{n+1})$ by the prediction

$$C_\alpha(f_{n+1}) = \{\Gamma_\theta(f_{n+1}) + r : r \in D_\alpha^\Phi(f_{n+1})\} \quad (10)$$

as with Local Conformal Prediction (LCP) [13] and Randomized LCP (RLCP) [15] prediction sets.

Algorithm 1 Local Spectral Conformal Inference

Input: $\mathcal{D}_{tr}, \mathcal{D}_{cal}, \Gamma_\theta, \Phi, D^\Phi, H, \alpha$, and f_{n+1}

1. Train the operator model: $\hat{\theta} := \arg \min_\theta \mathcal{L}(\Gamma_\theta, \mathcal{D}_{tr})$
 2. Calculate the weights based on the localization kernel: $w_t = H(f_t, f_{n+1})$ for all $f_t \in \mathcal{D}_{cal}$
 3. Calculate the local calibration scores: $D^\Phi(r_t) = \inf_\phi D(\phi(r_t) \mid \phi(G_{n+1}))$, where $r_t = g_t - \Gamma_{\hat{\theta}}(f_t) \quad \forall (f_t, g_t) \in \mathcal{D}_{cal}$
 4. Threshold q_{n+1} as the $\lceil(1 - \alpha)(n + 1)\rceil$ smallest $D^\Phi(r_t)$ value
- Return:** $C_\alpha(f_{n+1}) = \{\Gamma_{\hat{\theta}} + r : \forall r \in \mathcal{G} \text{ s.t. } D^\Phi(r) \geq q_{n+1}\}$
-

Algorithm 1 summarizes the LSCI procedure for generating statistically guaranteed prediction sets for operator models. The power of this approach is that we get exact prediction sets on the functional distribution G_{n+1} using only locally weighted univariate measures $\phi(G_{n+1})$. We theoretically show that these sets achieve exact marginal coverage (Section 3.3), while being highly adaptive in practice (Section 4) under a wide range of localizers and depth measures.

3.3 Theory

As an uncertainty quantification (UQ) technique, it is essential that our generated prediction sets guarantee coverage. However, localization (Equation 8) breaks exchangeability, which invalidates the validity guarantee of standard conformal methods (Equation 3). Recently, [2] showed that the coverage gap of non-exchangeable methods can be upper bounded as

$$P(g_{n+1} \in C_\alpha(f_{n+1})) \geq 1 - \alpha - \sum_{t=1}^n w_t d_{TV}(R, R^t) \quad (11)$$

where w_1, \dots, w_n are the localization weights, $R = \{r_1, \dots, r_{n+1}\}$ are the calibration, plus unknown test, residuals, R^t is R permuted so that r_t and r_{n+1} are swapped, and $d_{TV}(\cdot)$ is the total variation distance. If the data are fully exchangeable, then $d_{TV}(R, R^t) = 0$, and hence coverage is exact. At the other extreme, if $d_{TV}(R, R^t) = 1$, the max value, then coverage is vacuously bounded below by $-\alpha < 0$. Thus, this bound is not overly helpful unless we can quantify the degree of non-exchangeability.

Local exchangeability While our localization function $H(f_t, f_{n+1})$ breaks exchangeability, it also encodes the assumption that if two covariates f_t and f_{n+1} are close, then their prediction residuals, r_t and r_{n+1} , are close in distribution. We formally characterize this as a type of local exchangeability assumption [8] (Reviewed in Section A.1). Local exchangeability states that two residuals r_t and r_s are closer to exchangeable the closer f_t and f_s are to each other, i.e. that while the distribution of the residuals changes over time, it also evolves continuously as a function of the inputs.

Under local exchangeability, we can provide a non-vacuous bound on the coverage gap. Proposition 3.1 shows that the coverage gap of the prediction sets shrinks with the bandwidth.

Proposition 3.1. *If the data are locally exchangeable under the pre-metric $d : \mathcal{F} \times \mathcal{F} \mapsto \mathbb{R}^+$, then the coverage gap of LSCI is bounded above as*

$$\sum_{i=1}^n w_i d_{TV}(R, R^i) \leq \frac{\sum_{t=1}^n \exp(-\lambda d_t) d_t}{\sum_{t=1}^{n+1} \exp(-\lambda d_t)} \quad (12)$$

where $d_t = d(f_t, f_{n+1})$ and assuming an exponential localization weights $w_t \propto \exp(-\lambda d_t)$.

Proof deferred to Section A.2. The bound in proposition 3.1 tell us how the coverage gap behaves as a function bandwidth λ and the “strength” of local exchangeability.

Selecting the bandwidth If we take $\lambda \rightarrow 0$, then the coverage gap reduces to $\sum_t d_t / (n+1)$. If the data are close to exchangeable, i.e. $d_t \approx 0 \forall t$, then coverage will be guaranteed and if the data are far from exchangeable, $d_t \approx 1$, then coverage is impossible. Conversely, if we take $\lambda \rightarrow \infty$, then the gap goes to zero assuming $d_{n+1} < d_t \forall t \in 1, \dots, n$, hence coverage will “guaranteed” regardless of exchangeability.

However, modifying λ also modifies the local CDF estimate (Equation 8), which can also impact coverage. Setting $\lambda \rightarrow 0$ causes $w_t \rightarrow 1/(n+1)$, the standard empirical CDF, which is too diffuse for localization. Setting $\lambda \rightarrow \infty$ causes $w_t \rightarrow 0$ for all weights except w_{n+1} . In that case, the CDF is a step function, which is too localized to capture the distribution and estimate quantiles. That is, all depth values will be 0 and not induce a useful ordering. Therefore, λ has to be chosen to balance coverage and localization. We resort to cross validation on the calibration set to choose a λ value for each problem, and show that the marginal coverage is not too sensitive to λ choice (Table 4.1).

3.4 Sampling the prediction set

Depth-based prediction sets (Equation 10) only exist as implicit subsets of the function space \mathcal{G} , which makes them difficult to apply in practice. For instance, they do not immediately yield a typical range over which the *graphs* of the functions $g \in \mathcal{G}$ might occur, i.e. a prediction band. Because the prediction set is infinitely large, we introduce a simple rejection-sampling scheme to approximate it over the graphs of the functions. We detail this procedure in Algorithm 2 below.

Algorithm 2 Inverse Transform Residual Sampling

Input: $D_\alpha^\Phi(f_{n+1})$, H , $M \geq 1$, $n_s \geq 1$
1. Estimate Φ as the first $k = 1, \dots, M$ locally weighted, $H(f_t, f_{n+1})$, FPCs of r_1, \dots, r_n
repeat
 while $k \leq M$ **do**
 2. Sample $u \sim U(0, 1)$
 3. Compute $\tilde{r}_k = \phi_k(G_{n+1})^{-1}(u)$
 end while
4. Accept $\tilde{r}_{n+1}^i = (\tilde{r}_1, \dots, \tilde{r}_M)$ if $\Gamma_{\hat{\theta}}(f_{n+1}) + \tilde{r} \in D_\alpha^\Phi(f_{n+1})$
until n_s samples accepted.
Return: $\{\tilde{r}_{n+1}^1, \dots, \tilde{r}_{n+1}^{n_s}\}$.

Algorithm 2 involves two primary steps. First, we estimate the local functional principal components Φ (citation) to roughly approximate the distribution of G_{n+1} . Then, we draw random samples from G_{n+1} using inverse transform sampling with the local empirical quantile functions $\phi_k(G_{n+1})^{-1}(u)$ along each local FPC ϕ_k in ϕ_1, \dots, ϕ_M . Finally, we check if the sampled residual function, \tilde{r}_{n+1}^i , is inside the central region $D_\alpha^\Phi(f_{n+1})$, which defines the prediction set $C_\alpha(f_{n+1})$. If it is, then we accept \tilde{r}_{n+1}^i and add it to the ensemble, otherwise we reject and start over.

Using Algorithm 2, we can explicitly construct an ensemble representation of the prediction set as

$$\tilde{C}_\alpha(f_{n+1}) = \{\Gamma_{\hat{\theta}}(f_{n+1}) + \tilde{r}_{n+1}^i : i \in 1, \dots, n_s\}, \quad (13)$$

where n_s is the number of accepted samples. Although Algorithm 2 is not a lightweight procedure, it is amenable to parallelization because sampling can be done in parallel or vectorized. We can further summarize $\tilde{C}_\alpha(f_{n+1})$ into a prediction band by finding the point-wise min and max over the domain.

3.5 Related work

Local Conformal Inference Local Conformal inference is a recent adaptive conformal inference approach that uses locally weighted CDFs / quantile functions to estimate instance-wise prediction sets [13, 2, 15]. LCP methods introduce a localizer function H , which measure how similar the new input f_{n+1} is to the calibration inputs f_1, \dots, f_n and weights the residual CDF appropriately. Our work can be viewed as an operator extension, and generalization, of Local Conformal Prediction (LCP) [13] and Randomized Local Conformal Prediction (RLCP) [15].

Adaptive scoring rules Adaptive scoring rules modify the scoring rule to account for heteroskedasticity. Adaptive scoring rules are reliant on our ability to train an extra model $\hat{\sigma}(\cdot)$. If the training data is reused to estimate $\hat{\sigma}(\cdot)$, then this can result in severe underestimation of the predictive variance [40]. We will compare our approach against functional variations of adaptive scoring, including [10], [23], and [35].

Conformalized Quantile Regression Conformalized Quantile Regression (CQR) is an alternative approach for adaptive prediction sets, which modulates the output of a quantile regression operator to have finite sample coverage [40]. As shown in [13], CQR based methods can struggle with high quantiles and result in overly wide prediction sets. We will compare our approach against functional variants including [29], [1], and [32].

4 Experiments

We first consider three synthetic examples using Gaussian processes – 1D regression, 1D autoregressive forecasting, and 2D Spherical autoregressive forecasting. Details of each data generating mechanism provided in Appendix A.3. For each problem, we use a four layer, 64 channel Fourier Neural Operator (FNO) [24] with 16 Fourier modes for the 1D problems, and 16×32 modes for the 2D problem. Each model is trained for 50 epochs using adam [18] with a learning rate of 0.001.

We measure the empirical risk control [3] and width of the resulting prediction sets. The risk of a prediction set is $R(C_\alpha) = P(\int_D 1(g_{n+1}(t) \in C_\alpha(f_{n+1})(t))dt \geq 1 - \delta)$ where δ controls how much the target g_{n+1} is allowed to exceed the bounds of the prediction set while still being considered “covered”. We will use $\delta = 0.01$ to allow 1% of g_{n+1} to be outside $C_\alpha(f_{n+1})$ for the 1D problems and $\delta = 0.001$ for the 2D problem. The width is defined as the median distance between pointwise upper and lower bounds of $C_\alpha(f_{n+1})$. We also measure the distance correlation [45] between the loss defining the risk (and the width of the prediction set), with the true prediction error variance to assess the empirical adaptivity of each approach.

4.1 Synthetic experiments

We first show that the marginal coverage guarantee (Proposition 3.1) holds under a range of projection schemes Φ , depth notions D , localizer functions H , and kernel bandwidths for the localizers.

Different Φ projectors We will consider randomized slice sampling (Rand), Functional Principle Components (FPCA), a wavelet decomposition (Wave), FPCA + slice sampling (R-FPCA) wavelets + slice sampling (R-Wave) for Φ . For the base univariate depth functions (Equation 5), we include Tukey depth, ℓ_∞ -depth, and Mahalanobis depth, representing Type A, B, and C depth constructions [53], respectively. We apply each method to 1D Gaussian process regression problem with heteroskedastic variance and measure the marginal coverage over 100 simulation replicates.

Table 4.1a shows that LSCI nearly achieves the nominal coverage ($\alpha = 0.1$) under all combinations of projection schemes and depth notions. Adding randomization to a data driven (FPCA) or fixed (Wave) projection scheme slightly improves empirical coverage. Table 4.1a also confirms that the coverage gap (Proposition 3.1) is small in practice.

Different H localizers We next evaluate the marginal coverage of LSCI under three localizers: an ℓ_2 kernel $H(f_t, f_s) = \exp(-\lambda \|f_t - f_s\|_2)$, an ℓ_∞ kernel $H(f_t, f_s) = \exp(-\lambda \|f_t - f_s\|_\infty)$ and a k nearest neighbor kernel where $k = (1 + \lambda)^{-1}n$. The bandwidth $\lambda \geq 0$ controls the degree of

	Tukey	ℓ_∞ -Norm	Mahal.		ℓ_2	ℓ_∞	k-NN
Rand	0.902 \pm 0.02	0.905 \pm 0.01	0.904 \pm 0.02	$\lambda = 1$	0.903 \pm 0.02	0.903 \pm 0.01	0.905 \pm 0.01
FPCA	0.902 \pm 0.01	0.906 \pm 0.01	0.908 \pm 0.01	$\lambda = 2$	0.904 \pm 0.02	0.904 \pm 0.02	0.902 \pm 0.02
Wave	0.905 \pm 0.01	0.903 \pm 0.01	0.902 \pm 0.01	$\lambda = 3$	0.904 \pm 0.02	0.905 \pm 0.02	0.904 \pm 0.01
R-FPCA	0.901 \pm 0.02	0.901 \pm 0.02	0.901 \pm 0.01	$\lambda = 4$	0.904 \pm 0.02	0.904 \pm 0.02	0.903 \pm 0.02
R-Wave	0.904 \pm 0.02	0.905 \pm 0.02	0.903 \pm 0.02	$\lambda = 5$	0.904 \pm 0.02	0.903 \pm 0.02	0.903 \pm 0.02

(a) Coverage ($\alpha = 0.1$) by depth D and projection family Φ with 2σ error bars.

(b) Coverage ($\alpha = 0.1$) by localizer H and bandwidth λ with 2σ error bars.

localization. Table 4.1b shows that LSCI achieves nominal *marginal* coverage for all localizers across a range of bandwidths.

Comparison against baselines Next, we compare our proposed approach against baseline conformal inference methods for operator models on the three synthetic GP prediction tasks. We consider the following baselines: standard low-rank conformal prediction sets for functional data [23], band depth based conformal inference [10], two operator variants of conformalized quantile regression ([29] and [32]), and an adaptive functional scoring rule [35]. We do not include standard heuristics such as MC-Dropout, Deep Ensembles, and Laplace approximations due to their computational inefficiency and poor performance relative to conformal methods for operator models [29, 32]. For our proposed method we will include four variants: LSCI1 ($n_\phi = 20, H = \ell_2$), LSCI2 ($n_\phi = 20, H = \ell_\infty$), LSCI3 ($n_\phi = 100, H = \ell_2$), and LSCI4 ($n_\phi = 100, H = \ell_\infty$). Each method uses Tukey depth, and the localizer’s λ values were set via cross validation on the calibration set.

Method	Reg-GPID				AR-GPID				AR-SGP2D			
	Risk \uparrow	dCR \downarrow	Width \downarrow	dCW \uparrow	Risk \uparrow	dCR \downarrow	Width \downarrow	dCW \uparrow	Risk \uparrow	dCR \downarrow	Width \downarrow	dCW \uparrow
<i>Baselines</i>												
Conf1	0.675	0.238	1.210	0.000	0.812	0.179	1.183	0.000	0.674	0.599	0.919	0.000
Conf2	0.733	0.215	1.256	0.000	0.861	0.143	1.226	0.000	0.801	0.477	1.047	0.000
Supr.	0.893	0.111	1.560	0.000	0.910	0.098	1.347	0.000	0.949	0.302	1.226	0.000
UQ-NO	0.964	0.020	3.677	0.212	0.964	0.021	5.115	0.204	0.510	0.503	0.805	0.213
Pr-NO	0.057	0.043	0.672	0.993	0.339	0.007	0.590	0.989	0.016	0.325	0.503	0.997
Qt-NO	0.591	0.084	1.711	0.215	0.677	0.060	2.252	0.203	0.910	0.071	1.614	0.329
<i>Proposed</i>												
LSCI1	0.918	0.011	1.456	0.962	0.923	0.028	1.043	0.961	0.963	0.125	0.866	0.990
LSCI2	0.903	0.022	1.432	0.982	0.919	0.037	1.014	0.986	0.960	0.113	0.838	0.995
LSCI3	0.916	0.005	1.488	0.969	0.942	0.015	1.081	0.957	0.972	0.091	0.880	0.989
LSCI4	0.921	0.013	1.461	0.968	0.924	0.033	1.016	0.985	0.965	0.094	0.847	0.993

Table 1: Uncertainty metrics (risk, width, and distance correlation between risk/width and the true error variance) on synthetic Gaussian process simulations

Table 1 shows that the sampled LSCI prediction sets have appropriate risk control, low risk correlation, smallest widths, and high width correlations. This finding holds under a range of LSCI localizers, depths, and projection schemes.

4.2 Experiments on real data

We evaluate our approach against the same baselines in Section 4.1 on three real-world tasks. **Air quality** data includes hourly air pollutants data an air-quality monitoring site in Beijing, China from March 1st, 2013 to February 28th, 2017. **Energy Demand** data comes from the Energy Reliability Council of Texas (ERCOT) and contains daily, 24 hour demand curves, showing how much aggregate energy in kWh was used in Texas each hour between July 1st, 2015 and Feb. 19th, 2025. Finally, **Weather-ERA5** data includes global 2-meter surface temperature estimates interpolated onto a 32×64 latitude-longitude grid and aggregated into daily averages.

Table 2 shows the UQ metrics for each of the three datasets. In all cases, LSCI yields tighter prediction sets as measured by the coverage gap and width. Adaptivity measures (dCR and dCW) are less

Method	Air Quality				Energy Demand				Weather-ERA5			
	Risk \uparrow	dCR \downarrow	Width \downarrow	dCW \uparrow	Risk \uparrow	dCR \downarrow	Width \downarrow	dCW \uparrow	Risk \uparrow	dCR \downarrow	Width \downarrow	dCW \uparrow
<i>Baselines</i>												
Conf1	0.954	0.361	0.539	0.000	0.926	0.343	2.552	0.000	1.000	0.000	7.589	0.000
Conf2	0.962	0.308	0.537	0.000	0.941	0.311	2.533	0.000	1.000	0.000	7.543	0.000
Supr.	0.943	0.404	0.672	0.000	0.887	0.495	2.447	0.000	1.000	0.000	8.144	0.000
UQ-NO	0.985	0.152	0.632	0.200	0.979	0.108	3.060	0.430	1.000	0.000	10.30	0.017
Pr-NO	0.644	0.416	0.254	0.144	0.440	0.239	0.784	0.520	0.981	0.000	6.320	0.005
Qt-NO	0.962	0.343	0.443	0.197	0.875	0.298	2.618	0.216	0.733	0.151	3.234	0.080
<i>Proposed</i>												
LSCI1	0.931	0.220	0.401	0.199	0.906	0.384	1.799	0.492	0.950	0.023	5.443	0.008
LSCI2	0.916	0.229	0.383	0.197	0.900	0.404	1.816	0.465	0.980	0.009	5.658	0.004
LSCI3	0.939	0.247	0.399	0.184	0.906	0.386	1.813	0.504	0.945	0.023	5.387	0.008
LSCI4	0.916	0.212	0.382	0.188	0.903	0.378	1.757	0.480	0.979	0.011	5.654	0.003

Table 2: Uncertainty metrics (risk, width, and distance correlation between risk/width and the estimated error variance on real datasets)

informative than in Table 1 because heteroskadisticity, in these examples, comes from mixing a variety of differently shaped functions, rather than simply increasing or decreasing the error variance.

4.3 Spatial adaptivity

We further demonstrate the adaptivity of LSCI prediction sets by examining the sampled prediction bands over space. Figure 2 shows the generated upper and lower 90% LSCI band *on the residual process* (Equation 9) across four seasons of the Weather-ERA5 data. The bands clearly exhibit spatially varying seasonality, with the northern and southern hemispheres accurately flipping throughout the year. Thus, the bands are able to account for seasonal variations that the base FNO model was not able to represent.

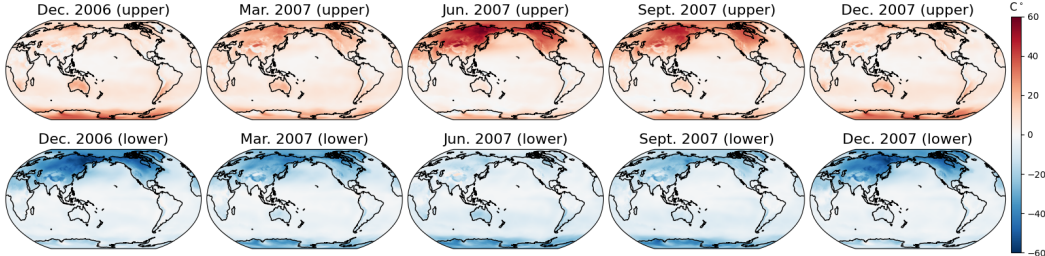


Figure 2: Spatial uncertainty as a function of seasonality. LSCI adapts over time to the true seasonal process.

5 Discussion

We introduced Local Sliced Conformal Inference (LSCI), a new framework for generating function-valued, locally adaptive prediction sets for black-box operator models. By leveraging projection-based Φ -depths and localized conformal calibration, LSCI captures the underlying structure and variability of operator residuals, while maintaining distribution-free coverage guarantees. Our theoretical results ensure both finite-sample marginal coverage and asymptotic conditional validity under local exchangeability assumptions. Empirical evaluations on synthetic and real-world operator tasks demonstrate that LSCI consistently outperforms existing conformal baselines in terms of both adaptivity and prediction set efficiency.

While LSCI offers strong theoretical and empirical performance, it comes with computational overhead due to the need for localization and sampling at test time. This makes the method less suited for fast or online inference without further optimization. Future work could explore amortized localizers, learned projection families, or variational approximations to accelerate sampling. In addition, extending LSCI to handle multivariate outputs with shared structure or applying it to probabilistic neural operators could broaden its scope and impact in scientific machine learning.

References

- [1] Anastasios N Angelopoulos, Amit Pal Kohli, Stephen Bates, Michael Jordan, Jitendra Malik, Thayer Alshaabi, Srigokul Upadhyayula, and Yaniv Romano. Image-to-image regression with distribution-free uncertainty quantification and applications in imaging. In *International Conference on Machine Learning*, pages 717–730. PMLR, 2022.
- [2] Rina Foygel Barber, Emmanuel J Candes, Aaditya Ramdas, and Ryan J Tibshirani. Conformal prediction beyond exchangeability. *The Annals of Statistics*, 51(2):816–845, 2023.
- [3] Stephen Bates, Anastasios Angelopoulos, Lihua Lei, Jitendra Malik, and Michael Jordan. Distribution-free, risk-controlling prediction sets. *Journal of the ACM (JACM)*, 68(6):1–34, 2021.
- [4] Jose Antonio Lara Benitez, Takashi Furuya, Florian Faucher, Anastasis Kratsios, Xavier Tricocche, and Maarten V de Hoop. Out-of-distributional risk bounds for neural operators with applications to the helmholtz equation. *Journal of Computational Physics*, 513:113168, 2024.
- [5] Philippe C Besse and Hervé Cardot. Approximation spline de la prévision d’un processus fonctionnel autorégressif d’ordre 1. *Canadian Journal of Statistics*, 24(4):467–487, 1996.
- [6] Kaushik Bhattacharya, Bamdad Hosseini, Nikola B Kovachki, and Andrew M Stuart. Model reduction and neural networks for parametric pdes. *The SMAI journal of computational mathematics*, 7:121–157, 2021.
- [7] Boris Bonev, Thorsten Kurth, Christian Hundt, Jaideep Pathak, Maximilian Baust, Karthik Kashinath, and Anima Anandkumar. Spherical fourier neural operators: Learning stable dynamics on the sphere. In *International conference on machine learning*, pages 2806–2823. PMLR, 2023.
- [8] Trevor Campbell, Saifuddin Syed, Chiao-Yu Yang, Michael I Jordan, and Tamara Broderick. Local exchangeability. *arXiv preprint arXiv:1906.09507*, 2019.
- [9] Tianping Chen and Hong Chen. Universal approximation to nonlinear operators by neural networks with arbitrary activation functions and its application to dynamical systems. *IEEE transactions on neural networks*, 6(4):911–917, 1995.
- [10] Jacopo Diquigiovanni, Matteo Fontana, and Simone Vantini. Conformal prediction bands for multivariate functional data. *Journal of Multivariate Analysis*, 189:104879, 2022.
- [11] Frédéric Ferraty, Aldo Goia, Enersto Salinelli, and Philippe Vieu. Recent advances on functional additive regression. *Recent advances in Functional Data Analysis and related topics*, pages 97–102, 2011.
- [12] Ramón Giraldo, Pedro Delicado, and Jorge Mateu. Continuous time-varying kriging for spatial prediction of functional data: An environmental application. *Journal of agricultural, biological, and environmental statistics*, 15:66–82, 2010.
- [13] Leying Guan. Localized conformal prediction: A generalized inference framework for conformal prediction. *Biometrika*, 110(1):33–50, 2023.
- [14] Trevor Harris, J Derek Tucker, Bo Li, and Lyndsay Shand. Elastic depths for detecting shape anomalies in functional data. *Technometrics*, 63(4):466–476, 2021.
- [15] Rohan Hore and Rina Foygel Barber. Conformal prediction with local weights: randomization enables local guarantees. *arXiv preprint arXiv:2310.07850*, 2023.
- [16] Andrada E Ivanescu, Ana-Maria Staicu, Fabian Scheipl, and Sonja Greven. Penalized function-on-function regression. *Computational Statistics*, 30:539–568, 2015.
- [17] Peishi Jiang, Zhao Yang, Jiali Wang, Chenfu Huang, Pengfei Xue, TC Chakraborty, Xingyuan Chen, and Yun Qian. Efficient super-resolution of near-surface climate modeling using the fourier neural operator. *Journal of Advances in Modeling Earth Systems*, 15(7):e2023MS003800, 2023.

- [18] Diederik P. Kingma and Jimmy Ba. Adam: A method for stochastic optimization. In *3rd International Conference on Learning Representations (ICLR)*, 2015.
- [19] Nikola Kovachki, Samuel Lanthaler, and Siddhartha Mishra. On universal approximation and error bounds for fourier neural operators. *Journal of Machine Learning Research*, 22(290):1–76, 2021.
- [20] Nikola B Kovachki, Samuel Lanthaler, and Andrew M Stuart. Operator learning: Algorithms and analysis. *arXiv preprint arXiv:2402.15715*, 2024.
- [21] Samuel Lanthaler, Zongyi Li, and Andrew M Stuart. The nonlocal neural operator: Universal approximation. *arXiv e-prints*, pages arXiv–2304, 2023.
- [22] Jing Lei, Max G’Sell, Alessandro Rinaldo, Ryan J Tibshirani, and Larry Wasserman. Distribution-free predictive inference for regression. *Journal of the American Statistical Association*, 113(523):1094–1111, 2018.
- [23] Jing Lei, Alessandro Rinaldo, and Larry Wasserman. A conformal prediction approach to explore functional data. *Annals of Mathematics and Artificial Intelligence*, 74:29–43, 2015.
- [24] Zongyi Li, Nikola Kovachki, Kamyar Azizzadenesheli, Burigede Liu, Kaushik Bhattacharya, Andrew Stuart, and Anima Anandkumar. Fourier neural operator for parametric partial differential equations. *arXiv preprint arXiv:2010.08895*, 2020.
- [25] Zongyi Li, Nikola Kovachki, Chris Choy, Boyi Li, Jean Kossaifi, Shourya Otta, Mohammad Amin Nabian, Maximilian Stadler, Christian Hundt, Kamyar Azizzadenesheli, et al. Geometry-informed neural operator for large-scale 3d pdes. *Advances in Neural Information Processing Systems*, 36:35836–35854, 2023.
- [26] Regina Y Liu. On a notion of data depth based on random simplices. *The Annals of Statistics*, pages 405–414, 1990.
- [27] Sara López-Pintado and Juan Romo. On the concept of depth for functional data. *Journal of the American statistical Association*, 104(486):718–734, 2009.
- [28] Lu Lu, Pengzhan Jin, Guofei Pang, Zhongqiang Zhang, and George Em Karniadakis. Learning nonlinear operators via deeponet based on the universal approximation theorem of operators. *Nature machine intelligence*, 3(3):218–229, 2021.
- [29] Ziqi Ma, Kamyar Azizzadenesheli, and Anima Anandkumar. Calibrated uncertainty quantification for operator learning via conformal prediction. *arXiv preprint arXiv:2402.01960*, 2024.
- [30] Andreas Maier, Harald Köstler, Marco Heisig, Patrick Krauss, and Seung Hee Yang. Known operator learning and hybrid machine learning in medical imaging—a review of the past, the present, and the future. *Progress in Biomedical Engineering*, 4(2):022002, 2022.
- [31] Mathew W McLean, Giles Hooker, Ana-Maria Staicu, Fabian Scheipl, and David Ruppert. Functional generalized additive models. *Journal of Computational and Graphical Statistics*, 23(1):249–269, 2014.
- [32] Amirhossein Mollaali, Gabriel Zufferey, Gonzalo Constante-Flores, Christian Moya, Can Li, Guang Lin, and Meng Yue. Conformalized prediction of post-fault voltage trajectories using pre-trained and finetuned attention-driven neural operators. *arXiv preprint arXiv:2410.24162*, 2024.
- [33] Karl Mosler. Depth statistics. *Robustness and complex data structures*, pages 17–34, 2013.
- [34] Karl Mosler and Yulia Polyakova. General notions of depth for functional data. *arXiv preprint arXiv:1208.1981*, 2012.
- [35] Christian Moya, Amirhossein Mollaali, Zecheng Zhang, Lu Lu, and Guang Lin. Conformalized-deeponet: A distribution-free framework for uncertainty quantification in deep operator networks. *Physica D: Nonlinear Phenomena*, 471:134418, 2025.

- [36] Stanislav Nagy, Irène Gijbels, Marek Omelka, and Daniel Hlubinka. Integrated depth for functional data: statistical properties and consistency. *ESAIM: Probability and Statistics*, 20:95–130, 2016.
- [37] Nicholas H Nelsen and Andrew M Stuart. The random feature model for input-output maps between banach spaces. *SIAM Journal on Scientific Computing*, 43(5):A3212–A3243, 2021.
- [38] Jaideep Pathak, Shashank Subramanian, Peter Harrington, Sanjeev Raja, Ashesh Chattopadhyay, Morteza Mardani, Thorsten Kurth, David Hall, Zongyi Li, Kamyar Azizzadenesheli, et al. Fourcastnet: A global data-driven high-resolution weather model using adaptive fourier neural operators. *arXiv preprint arXiv:2202.11214*, 2022.
- [39] James O Ramsay and CJ1125714 Dalzell. Some tools for functional data analysis. *Journal of the Royal Statistical Society Series B: Statistical Methodology*, 53(3):539–561, 1991.
- [40] Yaniv Romano, Evan Patterson, and Emmanuel Candes. Conformalized quantile regression. *Advances in neural information processing systems*, 32, 2019.
- [41] Benjamin Sandeise, Panos Stinis, Romit Maulik, and Shady E Ahmed. Scientific machine learning for closure models in multiscale problems: A review. *arXiv preprint arXiv:2403.02913*, 2024.
- [42] Igal Sason and Sergio Verdú. f -divergence inequalities. *IEEE Transactions on Information Theory*, 62(11):5973–6006, 2016.
- [43] Fabian Scheipl, Ana-Maria Staicu, and Sonja Greven. Functional additive mixed models. *Journal of Computational and Graphical Statistics*, 24(2):477–501, 2015.
- [44] Glenn Shafer and Vladimir Vovk. A tutorial on conformal prediction. *Journal of Machine Learning Research*, 9(3), 2008.
- [45] Gábor J Székely, Maria L Rizzo, and Nail K Bakirov. Measuring and testing dependence by correlation of distances. *The Annals of Statistics*, 35(6):2769–2794, 2007.
- [46] Tapas Tripura and Souvik Chakraborty. Wavelet neural operator for solving parametric partial differential equations in computational mechanics problems. *Computer Methods in Applied Mechanics and Engineering*, 404:115783, 2023.
- [47] Jane-Ling Wang, Jeng-Min Chiou, and Hans-Georg Müller. Functional data analysis. *Annual Review of Statistics and its application*, 3(1):257–295, 2016.
- [48] Min Wei and Xuesong Zhang. Super-resolution neural operator. In *Proceedings of the IEEE/CVF Conference on Computer Vision and Pattern Recognition*, pages 18247–18256, 2023.
- [49] Gege Wen, Zongyi Li, Qirui Long, Kamyar Azizzadenesheli, Anima Anandkumar, and Sally M Benson. Real-time high-resolution co₂ geological storage prediction using nested fourier neural operators. *Energy & Environmental Science*, 16(4):1732–1741, 2023.
- [50] Shuang Wu and Hans-Georg Müller. Response-adaptive regression for longitudinal data. *Biometrics*, 67(3):852–860, 2011.
- [51] Fang Yao and Hans-Georg Müller. Functional quadratic regression. *Biometrika*, 97(1):49–64, 2010.
- [52] Fang Yao, Hans-Georg Müller, and Jane-Ling Wang. Functional data analysis for sparse longitudinal data. *Journal of the American statistical association*, 100(470):577–590, 2005.
- [53] Yijun Zuo and Robert Serfling. General notions of statistical depth function. *Annals of statistics*, pages 461–482, 2000.

A Appendix / supplemental material

A.1 Local Exchangeability

Let $(Y_t)_{t \in \mathcal{T}}$ denote a stochastic process on \mathbb{R} with finite first and second moments. $(Y_t)_{t \in \mathcal{T}}$ is exchangeable if

$$(Y_t)_{t \in \mathcal{T}} =_D (Y_t)_{\pi(t) \in \mathcal{T}},$$

for all injective maps $\pi : \mathcal{T} \mapsto \mathcal{T}$, i.e. for all permutations of the indexing set [8]. Exchangeability means that re-ordering $(Y_t)_{t \in \mathcal{T}}$ along \mathcal{T} does not change its distribution. Exchangeability is ordinarily required to prove the finite sample validity of conformal prediction sets, which are based on the adjusted quantiles of the empirical measure.

Local exchangeability is a recent generalization of exchangeability that assumes $(Y_t)_{t \in \mathcal{T}}$ is not exchangeable, but that elements close in the indexing set are close to exchangeable. $(Y_t)_{t \in \mathcal{T}}$ is locally exchangeable in \mathcal{T} if for any subset $T \subset \mathcal{T}$ and injective map $\pi : T \mapsto \mathcal{T}$

$$d_{TV}(Y_T, Y_{\pi(T)}) \leq \sum_{t \in T} d(t, \pi(t)) \quad (14)$$

where Y_T is $(Y_t)_{t \in \mathcal{T}}$ restricted to T , $Y_{\pi(T)}$ is $(Y_t)_{t \in \mathcal{T}}$ restricted to $\pi(T)$, d_{TV} is the total variation distance [42], and $d : \mathcal{T} \mapsto \mathcal{T}$ is a pre-metric on \mathcal{T} .

Local exchangeability is critical because, while each Y_τ , $\tau \in \mathcal{T}$, follows its own distribution G_τ , we can approximate G_τ with a local empirical measure

$$\hat{G}_\tau = \sum_{t \in \mathcal{T}} \eta_t(\tau) \delta(Y_t) \quad (15)$$

where $\delta(Y_t)$ is an indicator function and $\eta_t(\tau)$ are localization weights. These weights are defined as

$$\eta_t(\tau) = \max\{0, M_\tau^{-1} + 2(\mu_\tau - d(t, \tau))\}$$

$$M_\tau = \max_M \left\{ \left(M^{-1} \sum_{t=1}^M (1 + 2d_m(\tau)) \right) \geq 2d_M(\tau) \right\}, \quad \mu_\tau = M_\tau^{-1} \sum_{t=1}^{M_\tau} d(t, \tau) \quad (16)$$

where $m, M \in 1, \dots, T$ and $d_m(\tau)$ is the m 'th smallest distance. Thus, we can use the adjusted quantiles of the local empirical measure to construct a local conformal prediction set for each $Y_t \in (Y_t)_{t \in \mathcal{T}}$.

A.2 Proofs

Proof of proposition 3.1. Let $H : \mathcal{F} \times \mathcal{F} \mapsto \mathbb{R}$ denote an exponential localization kernel, i.e. $H(f_1, f_2) \propto \exp(-\lambda d(f_1, f_2))$ where $\lambda \geq 0$ controls the bandwidth and $d : \mathcal{F} \times \mathcal{F} \mapsto \mathbb{R}$ is a bounded pre-metric on \mathcal{F} . Without loss of generality we assume $0 \leq d(f_1, f_2) \leq 1$. The coverage gap in proposition 3.1 and equation 11 is defined as

$$\sum_{t=1}^n w_t d_{TV}(R, R^t), \quad (17)$$

where $R = \{r_t = g_t - \Gamma_{\hat{\theta}}(f_t) : (f_t, g_t) \in \mathcal{D}_{cal}\}$ and R^t is the set R under the permutation function $\pi : T \mapsto T$, which swaps r_t with r_{n+1} , and leaves all other elements unchanged. By the definition of local exchangeability (Definition 14)

$$\sum_{t=1}^n w_t d_{TV}(R, R^t) \leq \sum_{t=1}^n w_t \sum_{i=1}^n d(f_i, f_{\pi(i)}). \quad (18)$$

However, because $d(f_i, f_{\pi(i)}) = 0$ for all $i \neq t$ since $i = \pi(i)$ in this case, the upper bound reduces to $\sum_{t=1}^n w_t d(f_t, f_{n+1})$. For notational convenience, we let $d_t = d(f_t, f_{n+1})$ and write

$$\sum_{t=1}^n w_t \sum_{i=1}^n d(f_i, f_{\pi(i)}) = \sum_{t=1}^n w_t d_t. \quad (19)$$

Substituting the definition of $w_t = \exp(-\lambda d_t) / \sum_{t=1}^{n+1} \exp(-\lambda d_t)$ into the above equation, we get the final inequality

$$\sum_{t=1}^n w_t d_{tv}(R, R^t) \leq \frac{\sum_{t=1}^n \exp(-\lambda d_t) d_t}{\sum_{t=1}^{n+1} \exp(-\lambda d_t)} \quad (20)$$

for any bandwidth value $\lambda \geq 0$.

A.3 Simulation details

We generate the Gaussian process data in Section 4.1 as follows.

1D regression We sample $n_{train} = 1000$ functional regression pairs $\{(f_t, g_t)\}$ according to the following data generating mechanism

$$\begin{aligned} f_t(x) &\sim \mu_t(x) + \sigma_x GP \\ g_t(x) &\sim (f_t * \beta)(x) + \sigma_t GP. \end{aligned}$$

to first train the FNO model. Here the mean function $\mu_t(x) = 2 \sin(t) \sin(2\pi x)$, and the two variance functions are $\sigma_x = 0.1$, and $\sigma_t(x) = 0.1(1.25 + \sin(t))$. We let $x \in [0, 1]$ and $t \in [-2\pi, 2\pi]$. The kernel defining the β function is given by $[-2, -1, 0, 1, 2]$, which is convolved as a sliding window over each f_t . Thus, this process is locally exchangeable (Section A.1). The GP noise in each process is sampled as 21 Fourier basis functions with $N(0, 1/k)$ random coefficients, where $k = 1, \dots, 21$ is the frequency number. We then sample $n_{cal} = 1000$ pairs to estimate the LSCI prediction sets, and $n_{test} = 1000$ to check the out of sample coverage and width.

1D Autoregression We generate a sequence of $n_{train} = 1001$ functional observations, i.e. a functional time series, according to the following data generating mechanism

$$g_t(x) \sim \mu_t(x) + \sigma_t GP$$

Here the mean function $\mu_t(x) = 2 \sin(t) \sin(2\pi x)$, and the two variance functions are $\sigma_x = 0.1$, and $\sigma_t(x) = 0.1(1.25 + \sin(t))$. We let $x \in [0, 1]$ and $t \in [-2\pi, 2\pi]$. Thus, this process is locally exchangeable (Section A.1). The GP noise in each process is sampled as 21 Fourier basis functions with $N(0, 1/k)$ random coefficients, where $k = 1, \dots, 21$ is the frequency number. We define an autoregressive FNO model that takes g_{t-1} and predicts g_t . Using this mechanism we generate $n_{cal} = 1000$ pairs (g_{t-1}, g_t) to estimate the LSCI prediction sets, and $n_{test} = 1000$ to check the out of sample coverage and width.

2D Spherical Autoregression Finally, we sample the 2D spherical GP data (2D-SGP) as follows. We generate a sequence of $n_{train} = 1001$ functional observations, i.e. a functional time series, according to the following data generating mechanism

$$g_t(s_1, s_2) \sim \mu_t(x) + \sigma_t GP$$

where, this time, the GP noise is sampled using the Torch Harmonics package [7] as a 2D spherical GP on a sphere. The mean function is defined as $\mu_t(x) = 2 \sin(t) \sin(2\pi x)$, and the variance $\sigma_t(x) = 0.1(1.25 + \sin(t))$. We let $x \in \mathbb{S}^2$ and $t \in [-2\pi, 2\pi]$. Thus, this process is locally exchangeable (Section A.1). We define an autoregressive FNO model that takes g_{t-1} and predicts g_t . Using this mechanism we generate $n_{cal} = 1000$ pairs (g_{t-1}, g_t) to estimate the LSCI prediction sets, and $n_{test} = 1000$ to check the out of sample coverage and width.